Calculation of Raman-active modes in linear and zigzag phases of fullerene peapods

H. Chadli, A. Rahmani, and K. Sbai
Département de Physique, Université MY Ismail, Faculté des Sciences, Boîte Postale 11201, Zitoune, 50000 Meknès, Morocco

P. Hermet, S. Rols, and J.-L. Sauvajol
Laboratoire des Colloides, Verres et Nanomatériaux (UMR CNRS 5587), CC026, Université Montpellier II, 34095 Montpellier Cedex 5, France

(Received 28 July 2006; revised manuscript received 19 September 2006; published 10 November 2006)

We report on minimum energy calculations, using a convenient Lennard-Jones expression of the van der Waals intermolecular potential, to derive the optimum configurations of C_{60} molecules inside single wall carbon nanotubes. Depending on the diameter of the nanotube, C_{60} molecules were found to form linear or zigzag chains inside the nanotubes. In the following, we use the spectral moments method, together with a bond-polarizability model, to calculate the nonresonant Raman spectrum for infinitely long isolated C_{60} peapods. We present the evolution of the Raman spectrum as a function of the diameter and chirality of the nanotube. The changes of the Raman spectrum as a function of the configuration of the C_{60} molecules inside the nanotubes are identified. On the other hand, the effect of the filling factor on the Raman spectrum is analyzed. These predictions are useful to interpret the experimental Raman spectra of fullerene peapods.

DOI: 10.1103/PhysRevB.74.205412 PACS number(s): 63.22.+m, 78.30.Na

I. INTRODUCTION

Among the tremendous amount of technological and theoretical advances that result from the discovery of fullerene[1] are new ideas and paths of investigations. Carbon nanotubes,[2] in particular, are one of the direct results of fullerenes research and they carry many hopes for future technological advances due to their special one-dimensional (1D) nanosized structure. In particular, it has been suggested that their low mass over specific surface ratio could be used as nanohost for molecular energy storage. Many recent studies have shown that different atoms or molecules can be trapped inside the hollow core of a single-walled carbon nanotube (SWCNT).[3,4]

Fullerene peapods stand as supermolecular assemblies of C_{60} molecules inside SWCNTs (C_{60}@SWCNTs) and were first observed by Smith *et al.*[5] from transmission electron microscopy (TEM) experiments. In general, peapods are observed organized into bundles where they are packed together through van der Waals intertubes interactions, a structure that is clearly visible on TEM pictures.[6–8] Efforts led to the synthesis of high-quality 1D fullerene crystals inside SWCNT's.[5,6] These materials represent a new class of a hybrid system between C_{60} and SWCNT where the encapsulated C_{60} peas and the SWCNT pod are bonded through van der Waals interactions.

A lot of theoretical and experimental studies have been presented on peapods and several interesting properties have been predicted or observed. In particular, theoretical calculations predict that the electronic states near the Fermi level are substantially modified trough the C_{60}-SWCNT interaction.[9] Due to their tunable electronic properties, the potential applications of peapods range from high temperature superconductor[10] to memory element[11] and nanometer-sized container for chemical reactions.[12]

Raman spectroscopy has been shown to play a major role in nanotube science.[13] The Raman spectrum of SWCNT is dominated by the so-called radial breathing modes (RBM) below 350 cm^{-1} and by the tangential modes (TM) in the high wave number region (1400–1600 cm^{-1}). At a theoretical level, the nonresonant Raman spectra of SWCNTs have been calculated within the bond polarizability model.[14,15] Many experimental and theoretical Raman studies have shown that the RBM follow a straightforward dependence with the tube diameter that can be used to determine the distribution of the tube diameters in samples under study.[16] For the C_{60} molecule, a large variety of theoretical methods has been applied to the calculation of the internal modes and to the determination of their Raman activity.[17–22]

Total energy calculations of C_{60} peapods suggest that the smallest tube diameter for encasing C_{60} molecules inside SWCNT is around the diameter corresponding to (10,10) or (9,9) tubes.[23] Hodak and Girifalco have shown that the structure of the C_{60} molecules inside nanotubes is diameter dependent.[24,25] Therefore, it is interesting to follow the changes of the empty nanotubes properties, such as phonon modes, induced by C_{60} filling and also as a function of the fullerene configuration inside the nanotube. Few years ago, Raman experiments on SWCNTs encasing C_{60} molecules have been reported.[26,27] For tube diameters between 1.45 and 1.76 nm, the authors observed that the radial breathing-like mode (RBLM) frequencies is downshifted compared to the RBM of empty SWCNTs. For smaller diameters, close to 1.37 nm, they observed two RBLM components that are upshifted and downshifted with regards to the position of the RBM of the empty tube, respectively. Recently, Pfeiffer *et al.*[28] measured all the fundamental Raman lines of the encaged C_{60} peas except the $H_g(8)$ mode. They observed that both nondegenerate and totally symmetric A_g modes of C_{60} peas exhibit a splitting into two components. They attributed this splitting to the presence of both moving and static fullerenes inside the tubes.

In this paper, we present calculations of the nonresonant Raman spectrum of fullerene peapods by using the spectral

moments method. We focus on the radial breathing-like mode (RBLM) and tangential-like mode (TLM) ranges. These calculations have been performed for a large collection of nanotubes with various structural characteristics. In particular, for large nanotubes, the Raman spectra were calculated considering C_{60} molecules organized on a zigzag chain as this structure has been calculated to be energetically favorable for such tubes (see Sec. III A). Obviously, the Raman process in peapods is a resonant process. Consequently, our calculations do not predict the changes of the spectra with the excitation energy or the relative intensity of the different modes for a fixed excitation energy. Nevertheless, these calculations of the nonresonant Raman spectrum allow to investigate how the variation of the tube diameter, tube chirality, configuration of C_{60} molecules inside SWCNT and C_{60} filling factor influence the Raman spectrum. These predictions are useful to interpret the experimental Raman spectra of fullerene peapods.

II. COMPUTATIONAL METHOD

A carbon peapod consists of C_{60} molecules trapped inside a SWCNT host. The configuration of the guest molecules within the nanotube has already been found to be diameter dependent.[24,25] In this study, we consider SWCNTs with diameters ranging from 1.25 nm to 2.20 nm in which the C_{60} molecules phase can take a linear or a zigzag configuration depending on the diameter. The energy calculations were performed using a Lennard-Jones potential, $U_{\mathrm{LJ}}=4\epsilon[(\sigma/R)^{12}-(\sigma/R)^{6}]$, to describe the van der Waals interactions between both adjacent fullerene molecules and, on the other hand, between fullerenes and the nanotube. The values of the Lennard-Jones parameters were chosen as $\epsilon=2.964$ meV and $\sigma=0.3407$ nm. These values have recently been found to describe correctly the van der Waals contribution to the C_{60} bulk cohesive energy.[29] To derive the elements of the dynamical matrix, we used a van der Waals cutoff radius of 0.74 nm.

The C-C intratube interactions at the surface of the SWCNT are described by using the force constant model introduced by Saito,[14] and previously used to calculate the Raman spectra of isolated single wall carbon nanotubes with finite length.[15] The intramolecular interactions between carbon atoms at the surface of the C_{60} molecules are modelized by the force constants model described by Jishi and Dresselhaus.[22] In both nanotube and C_{60} force constants models, interactions up to the fourth nearest neighbors are accounted to derive the dynamical matrix.

In this paper, two types of calculations are presented.

(1) Total energy calculations and minimum energy structure will be discussed in Sec. III A. Only nanotubes with diameter D_t greater than 1.25 nm were considered. In order to obtain the optimal configuration of the C_{60} molecules inside the nanotubes, an energy minimization was performed with respect to six variable parameters: the distance between the centers of adjacent C_{60} molecules (d_{cc}), the distance between C_{60} center and the nanotube axis (d_{ct}), the relative Euler angles defining the orientation of the C_{60} molecules inside the tubes (α,β,γ), and a parameter defining the relative translation of the fullerene molecules along the tube axis (t_r) (see Fig. 1). In the present calculation, only the Lennard-Jones C_{60}-SWCNT and C_{60}-C_{60} interaction energies were minimized. In this procedure, we fix a certain supercell length for the nanotube and we introduce a number of C_{60} molecules (mostly four) inside the tube. Then the energy minimization is performed by varying the parameters cited above.

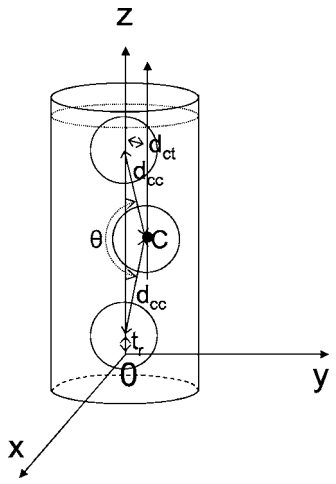

FIG. 1. Schematical representation of carbon peapods showing some of the parameters used for the geometrical optimization of the C_{60} molecules inside the nanotube (see text). The letter *C* indicates the position of the center of one of the C_{60} molecule.

The structural parameters derived from this procedure are used to build the dynamical matrix and then to calculate the Raman spectrum of C_{60}@SWCNT. For the calculations of the Raman spectrum, periodic conditions were applied to the supercells in order to simulate peapods of infinite length. For example, in the case of infinite C_{60}@(10,10) and C_{60}@(13,13) peapods, a portion of (10,10) [(13,13)] nanotube of length 3.94 nm (3.44 nm), respectively, is considered as a supercell. In those cases, the supercell contains four C_{60} molecules inside the tubes.

(2) The calculated Raman spectra will be presented in Sec. III B. The Raman scattering cross section can be calculated assuming the induced polarization tensor is known.[30] In this paper, the Raman cross section was calculated assuming that scattering can be described within the framework of the bond polarizability model. In that case, the polarization is only modulated by the nearest-neighbor bonds and the components of the induced polarizability tensor $\tilde{\pi}$ are given by the empiric equation[31,32]

$$\pi_{\alpha\beta}(r)=\tfrac{1}{3}(\alpha_l+2\alpha_p)\delta_{\alpha\beta}+(\alpha_l-\alpha_p)\left(\hat{r}_\alpha\hat{r}_\beta-\tfrac{1}{3}\delta_{\alpha\beta}\right), \quad (1)$$

where α and β relate to the Cartesian components (x,y,z) and $\hat{\vec{r}}$ is the unit vector along the vector $\vec{r}$ connecting atom n and atom m which are covalently bonded. The parameters α_l and α_p correspond to the longitudinal and perpendicular bond polarizability, respectively. Within this approach, one can assume that the bond polarizability parameters are functions of the bond lengths r only. The derivatives $\pi^n_{\alpha\beta,\gamma}$ are given by

TABLE I. The Raman polarizability parameter ($\bar{\alpha}$, $\bar{\beta}$, and $\bar{\gamma}$) for SWCNT and C_{60}.

		C_{60}	
	SWCNT	Single bond	Double bond
$\bar{\alpha}$ (in Å^2)	4.70	2.30	7.55
$\bar{\beta}$ (in Å^2)	4.00	2.30	2.60
$\bar{\gamma}$ (in Å^2)	0.04	1.28	0.32

$$\pi^n_{\alpha\beta,\gamma} = \sum_m \frac{1}{3}(2\alpha'_p + \alpha'_l)\delta_{\alpha\beta}\hat{r}_\gamma + (\alpha'_l - \alpha'_p)\left(\hat{r}_\alpha\hat{r}_\beta - \frac{1}{3}\delta_{\alpha\beta}\right)\hat{r}_\gamma + \frac{(\alpha_l - \alpha_p)}{r}(\delta_{\alpha\gamma}\hat{r}_\beta + \delta_{\beta\gamma}\hat{r}_\alpha - 2\hat{r}_\alpha\hat{r}_\beta\hat{r}_\gamma), \quad (2)$$

where $\alpha' = (\partial\alpha/\partial r)|_{r=r_0}$ and r_0 is the equilibrium bond distance.

In Table I, are given the values of the bond polarizability parameters

$$\bar{\alpha} = 2\alpha'_p + \alpha'_l, \quad \bar{\beta} = \alpha'_l - \alpha'_p \quad \text{and} \quad \bar{\gamma} = (\alpha_l - \alpha_p)/r$$

used in calculations.

When the system under study contains a large number of atoms, the dynamical matrix is very large and its diagonalization fails or requires long computing time. The spectral moment method appears as a very powerful method in such cases as it allows to compute directly the Raman spectra without diagonalizing the dynamical matrix.[33] The wave number of the Raman active modes are then directly obtained from the position of the peaks in the calculated Raman spectra.

In all our calculations, the nanotube axis is along the Z axis and a carbon atom of the SWCNT is along the X axis of the nanotube reference frame. The x, y, and z are the axes of the laboratory frame, and the laser beam is assumed to be along the y axis. In the VV configuration, both the incident and scattered polarizations are along the z axis. For the VH configuration, the incident and scattered polarizations are along the z and x axes, respectively. For oriented peapod, we considered the $Z(X)$ nanotube axis as being along the $z(x)$ axis ($VV \equiv ZZ$ and $VH \equiv ZX$). For unoriented peapod samples, an isotropic orientation of the tube axis is taken into account in the calculations of the VV and VH Raman spectra.

III. RESULTS

In a first section, we are interested in the geometric optimization of the C_{60} molecules in the tube for peapods of different diameters. Next, we report the results of calculated Raman spectra for infinite individual peapods. The dependence of the Raman spectrum as a function of the chirality and diameter of the nanotube, configuration of the C_{60} molecules inside the nanotube and average filling factor are considered.

TABLE II. Optimized structural parameters of the C_{60} molecules inside tube for different diameters and chiralities.

Tube index (n,m)	Tube diameter (nm)	C_{60}-tube distance (nm)	Angle θ (deg)	C_{60}-C_{60} distance (nm)
(10,10)	1.36	0.323	180	1.003
(15,4)	1.41	0.355	180	1.003
(11,11)	1.49	0.321	164	1.006
(18,4)	1.59	0.309	150	1.003
(12,12)	1.63	0.306	145	1.008
(21,0)	1.64	0.307	143	1.008
(15,10)	1.70	0.30	134	1.006
(22,0)	1.72	0.302	132	1.006
(13,13)	1.76	0.301	127	1.007
(23,0)	1.80	0.30	121	1.003
(18,9)	1.86	0.298	112	1.003
(14,14)	1.90	0.30	108	1.006
(25,0)	1.96	0.298	99	1.006
(19,10)	2.00	0.298	90	1.008
(15,15)	2.03	0.3025	88	1.004
(17,14)	2.11	0.296	70	0.998
(16,16)	2.17	0.297	60	1.0

A. Configuration of the C_{60} molecules inside the tube

In Table II we report the values of some of the structural parameters issued from the energy minimizations. The optimum fullerene packing can be characterized by the angle θ formed by three consecutive C_{60} (see Fig. 1). As an example, $\theta = 180°$ for a linear chain of fullerenes and zigzag chain will refer to a packing with $\theta < 180°$. This angle θ is found to depend primarily on the nanotube diameter and does not depend significantly on the chirality. We found that θ is 180° for tubes having a diameter lower than $D_c \approx 1.45$ nm and therefore the optimal positions of the C_{60} molecules occur when their centers are placed along the nanotube axis (linear chain). We found the linear chain as being optimum for tubes having a diameter $D_t = 2*(r_c + d)$, where r_c is the fullerene radius and d, the interlayer C_{60}-SWCNT distance, varies from 0.3 to 0.32 nm. These values of d are in agreement with the interlayer gaps commonly observed in carbon systems. In the following this peculiar configuration of peapod will be referred to as *linear peapod*. The perfect zigzag configuration ($\theta = 60°$) is reached for tubes with a diameter $D_t \approx 2.17$ nm. In the following the peapods in which the C_{60} molecules adopt a zigzag configuration ($\theta < 180°$) will be called *zigzag peapods*. Increasing the nanotube radius reduces the C_{60}-nanotube interaction and for the very large nanotube radius, the interaction energy should approach that of the fullerene with planar graphite. Using a semiclassical model, Hodak and Girifalco have shown that C_{60} molecules form a zigzag structure inside a (15,15) nanotube.[24] In this configuration they reported a value of the θ angle of 89°, a value in good agreement with the one reported in Table II. The optimal C_{60}-C_{60} gap is calculated around 0.99

−1.01 nm for all optimized peapods. This value is larger than the one deduced from diffraction profiles[34–36] (≃0.97 nm and 0.95 nm) and from TEM data.[37] However this shorter distance was associated to the presence of some polymerized phases of C_{60} inside the nanotubes which was also confirmed by recent spectroscopic studies.[38,39] Such phases have not been incorporated in our models.

B. The Raman spectrum of peapods

Most of the Raman experiments are performed on unoriented peapod samples. To make the comparison with the experimental results as realistic as possible, we performed an average of the Raman spectra over the nanotube orientations with regards to the laboratory frame. In Fig. 2 we present the *VV* and *VH* Raman spectra calculated for unoriented samples of (10,10) and (13,13) infinite SWCNTs and for their corresponding peapods: C_{60}@(10,10) (linear chain of C_{60} molecules) and C_{60}@(13,13) (zigzag configuration of C_{60} molecules) in the low-frequency (left-hand side) and high-frequency ranges (right-hand side). Calculations of the Raman spectrum for both linear and zigzag peapods show that the Raman active modes of the C_{60} do not depend on the tube chirality. We also found that there is no significant differences between the Raman spectra of the optimized and nonoptimized peapods in terms of relative angles of rotation and relative translations of the C_{60} molecules inside the tube.

Concerning the main modes of C_{60}, the $H_g(6)$, $H_g(7)$, $H_g(8)$, and $A_g(2)$ modes are located around 1220, 1403, 1583, and 1469 cm^{-1}, respectively, in C_{60}@(10,10) and C_{60}@(13,13), independently of the configuration of C_{60} molecules inside the tube. These modes show a small upshift (1–2 cm^{-1}) with respect to their positions in the free C_{60} spectrum. By contrast, the $A_g(1)$ and $H_g(2)$ modes of C_{60} are split in C_{60}@(10,10) [C_{60}@(13,13)] and the two components of each doublet are located at (498,511) cm^{-1} and (448,452) cm^{-1} [(495,506) cm^{-1} and (446,448) cm^{-1}], respectively. It can be pointed out that the splitting of the $A_g(1)$ and $H_g(2)$ modes were also obtained for a model consisting of a single C_{60} molecule capped inside a nanotube. This suggests that this splitting is related to the interactions between the C_{60} molecules and the nanotube host, and not to inter-C_{60} interactions. Finally, the $H_g(1)$ mode shows three components located at (275,282,289) cm^{-1} and (272,276,283) cm^{-1} in C_{60}@(10,10) and C_{60}@(13,13), respectively.

Concerning the main modes of SWCNT, we calculate that the TLM are almost not affected by the insertion of C_{60} molecules inside the nanotube. As already presented, the A_{1g} RBM, located at 165 and 127 cm^{-1} for the (10,10) and (13,13) SWCNTs, respectively, were observed in the *VV* configuration but vanished in the *VH* configurations.[15] The same behavior is observed for the RBLM in peapods, suggesting that the totally symmetric character of the RBM is conserved after insertion of C_{60}. A shift of the RBLM with regards to their RBM analogous is found. This shift depends on the configuration of the C_{60} molecules inside the nanotube. More precisely, insertion of C_{60} molecules inside the inner space of the tube induces a slight upshift of the RBLM mode when C_{60} molecules are organized as a linear chain. For instance, the RBLM shifts from 165 cm^{-1} in (10,10) tube to 170 cm^{-1} in C_{60}@(10,10) peapod (Fig. 2). On the other hand, for C_{60} molecules forming a zigzag chain, RBLM displays a double structure. For C_{60}@(13,13), this feature is made of a low-frequency component located at 125 cm^{-1}, downshifted with respect to the position of the RBM in the (13,13) SWCNT, and a high-frequency component at 133 cm^{-1} upshifted with respect to the RBM of the (13,13) SWCNT (Fig. 2).

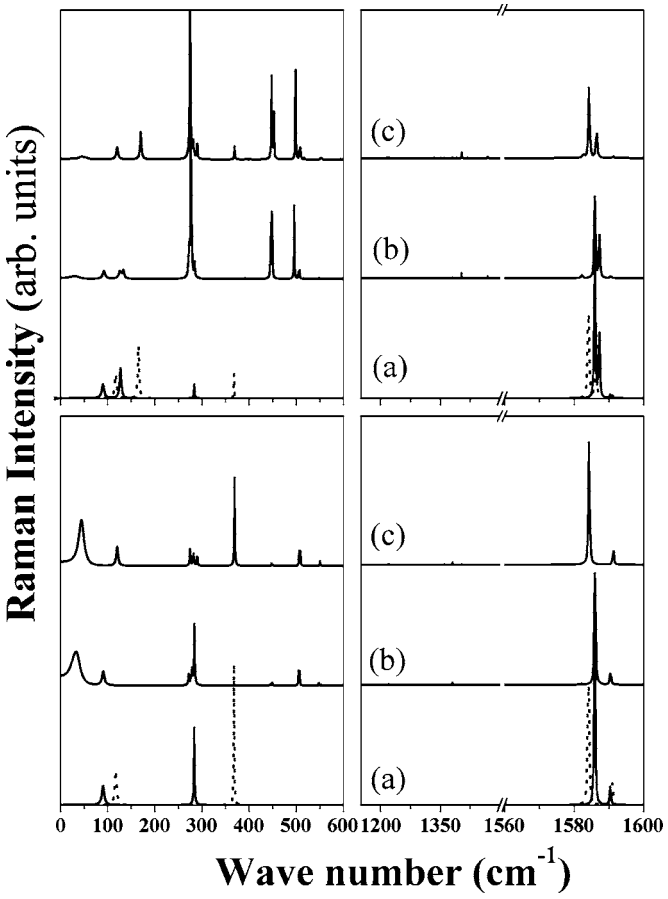

FIG. 2. The *VV* (top) and *VH* (bottom) calculated Raman spectra in the BLM (left) and TLM (right) ranges of peapods: C_{60}@(10,10) (curve *c*) and C_{60}@(13,13) (curve *b*). The calculated Raman spectra of the empty SWCNTs are displayed: (10,10) (curve *a*, dashed line) and (13,13) (curve *a*, solid line).

In the 600–1400 cm^{-1} intermediate-wave number region (not shown), a slight upshift (1–2 cm^{-1}) of the C_{60} modes and of the E_{2g} nanotube mode (located around 865 cm^{-1}) were found in peapod.

C. Diameter and chirality dependence of the Raman spectrum of peapods

In the following, Raman spectra have been calculated on individual oriented peapods. In this section, we focus on the BLM region of the $VV(\equiv ZZ)$ polarized Raman spectrum. We have investigated the dependence of some specific Raman-active modes of infinite peapods as a function of the diameter of the nanotube. Figure 3 shows the evolution of the RBM and RBLM frequencies as a function of the tube diam-

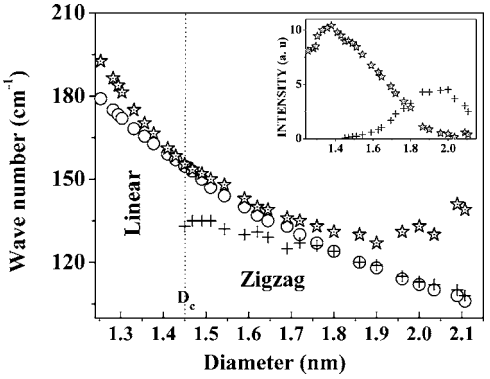

FIG. 3. The diameter dependence of the RBLM frequency in *linear* and *zigzag peapods*: high-frequency component, RBLM1, (star) and low-frequency component, RBLM2, (cross). The diameter dependence of the RBM for the related empty tubes is also displayed (open circles). The limit (D_c, see text) between *linear* and *zigzag peapods* is identified by the vertical dashed line. Inset: the corresponding intensities of the RBLM1 and RBLM2 versus the diameter of the nanotubes.

eter. The RBLM of linear (diameter below 1.45 nm) and zigzag (diameter between 1.45 and 2.17 nm) peapods show distinct behaviors. The behavior of the RBLM in linear peapods is qualitatively the same as those of the RBM. However, it deviates from the scaling law stated for the RBM frequency. For zigzag peapods, we already reported the splitting of the RBM into two components. For tubes having a diameter smaller than $D_0 \approx 1.78$ nm, associated to angles θ greater than $\theta_0 \approx 120°$, the high- and low-frequency component of RBLM doublet, called RBLM1 and RBLM2 in the following, downshift when the tube diameter increases. Note that the slopes of the variations are different. By contrast, for tubes having a diameter greater than $D_0 \approx 1.78$ nm, associated to angles θ lower than θ_0, the low (high)-frequency component of RBLM doublet downshifts (upshifts) when the diameter increases. In the inset of Fig. 3, we have reported the variation of the Raman intensities of the two components of the RBLM as a function of the nanotube diameter. The ratio $r = I_{\mathrm{RBLM1}}/I_{\mathrm{RBLM2}}$ is equal to 1 for $D \approx D_0$ ($\theta \approx \theta_0$), $r > 1$ for $D < D_0$ ($\theta > \theta_0$) and $r < 1$ for $D > D_0$ ($\theta < \theta_0$). When θ reaches 180° (60°), the ratio $r \gg 1$ ($r \ll 1$) and the low-frequency region is dominated by the component of the RBLM doublet located at the frequency the closest of the frequency of the RBM. The frequency and intensity behaviors of the RBLM1 and RBLM2 suggest an exchange from one mode to the other associated to an anticrossing effect of the dispersion curves of the RBLM1 and RBLM2 with the diameter in zigzag peapods.

We have also investigated the dependence of the Raman spectrum of peapods as a function of the chirality of the tube host. In this aim, we have calculated the $VV(\equiv ZZ)$ Raman spectra for infinite achiral (armchair and zigzag) and chiral peapods in both linear and zigzag phases. In Fig. 4 (top), we show the RBLM and TLM regions of the *VV* Raman spectrum for $C_{60}@(10,10)$, $C_{60}@(17,0)$, and $C_{60}@(14,5)$ *linear peapods* (the nanotube diameters are 1.35, 1.33, and 1.34 nm, respectively). For *zigzag peapods*, the Raman spectra were calculated for $C_{60}@(13,13)$, $C_{60}@(22,0)$, and

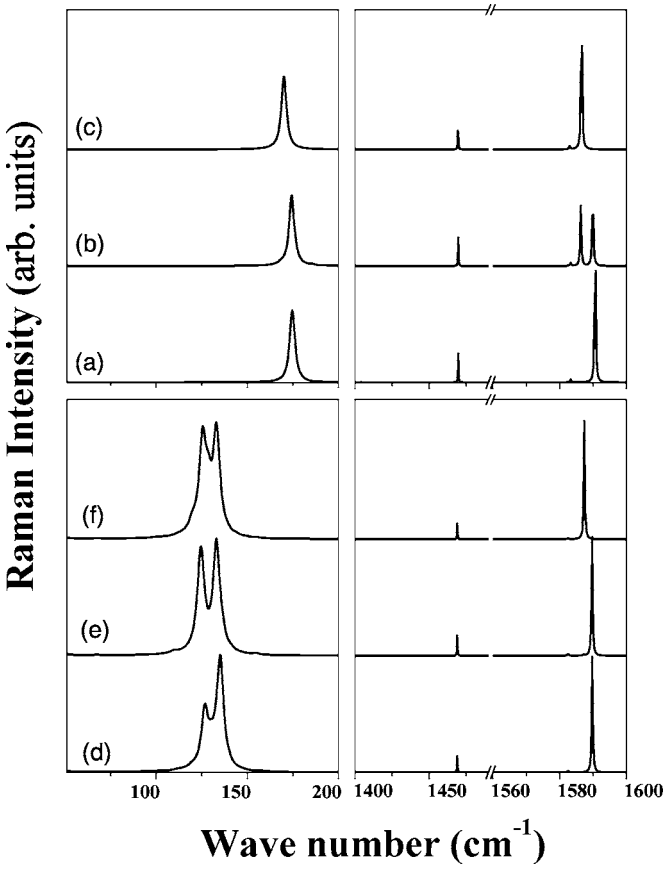

FIG. 4. Chirality dependence of the $VV(\equiv ZZ)$ polarized Raman spectrum. *Linear peapods* (top): $C_{60}@(17,0)$ (curve *a*), $C_{60}@(14,5)$ (curve *b*), $C_{60}@(10,10)$ (curve *c*). *Zigzag peapods* (bottom): $C_{60}@(22,0)$ (curve *d*), $C_{60}@(22,1)$ (curve *e*), and $C_{60}@(13,13)$ (curve *f*). Spectra are displayed in the BLM (left-hand side) and TLM (right-hand side) regions.

$C_{60}@(22,1)$ peapods (the tube diameters are 1.76, 1.72, and 1.76 nm, respectively) (Fig. 4, bottom). According to previous calculations for SWCNTs,[14,15] we found a chirality dependence of the TLM while the RBLM are mainly sensitive to the diameter of the tube. Concerning the RBLM modes, one observes that the linear phase is characterized by a single peak associated to the RBLM mode located at 170 cm^{-1} for $C_{60}@(10,10)$ and 174 cm^{-1} for $C_{60}@(14,5)$ and $C_{60}@(17,0)$. The BLM region of the Raman spectrum of zigzag peapods is characterized by a splitting of the RBLM into two modes located at (127,135), (126,135), and (125,133) cm^{-1} for $C_{60}@(22,0)$, $C_{60}@(22,1)$, and $C_{60}@(13,13)$, respectively. The RBM wave numbers are close to 127 cm^{-1} for (22,1) and (13,13) SWCNTs and 130 cm^{-1} for (22,0) SWCNT. The calculations show that the profile of the BLM region is slightly depending on chirality and strongly depends on the configuration of the C_{60} molecules inside the tube.

D. Dependence of Raman spectrum with the filling factor

In real peapod samples, it is reasonable to consider that all the nanotubes are not completely filled with C_{60}'s. The exact

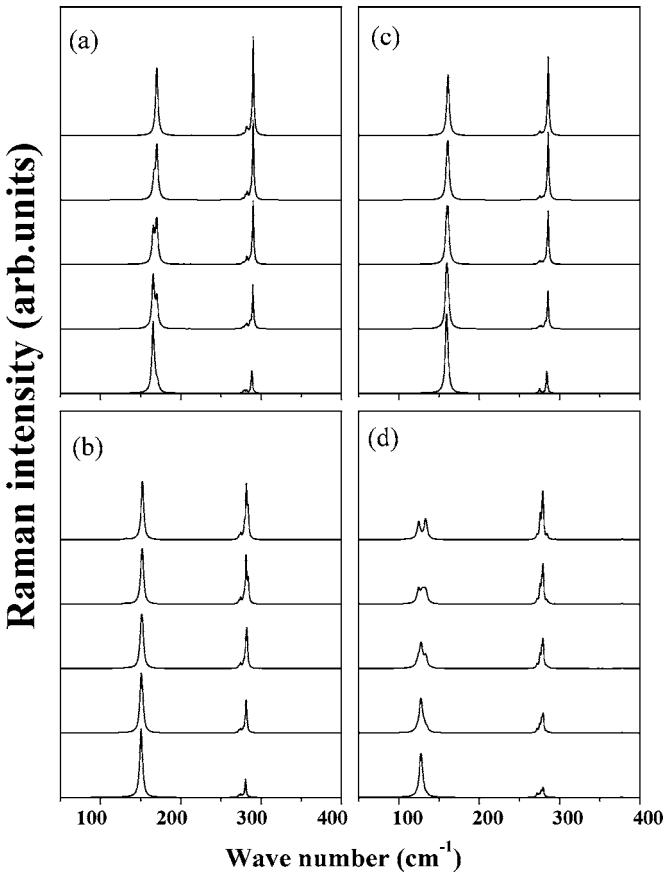

FIG. 5. The $VV(\equiv ZZ)$ polarized Raman spectra displayed in the BLM region of infinite peapods as a function of the filling factor. The filling factor is 20%, 40%, 60%, 80%, and 100% from bottom to top. *Linear peapods*: $C_{60}@(10,10)$ (curve *a*) and $C_{60}@(18,0)$ (curve *c*). *Zigzag peapods*: $C_{60}@(11,11)$ (curve *b*) and $C_{60}@(13,13)$ (curve *d*).

degrees of filling is still under discussion and ranges from a certain percent to almost 100% filling.[34,35] In this section, we make the hypothesis of partial filling of the tubes with a quasi-infinite long chain. This hypothesis is supported by observations reported in Ref. 35. Very long tubes are considered (more than 100 cells) and a defined number of C_{60} molecules are inserted. To avoid finite size effects, we applied periodic conditions to the tube. We found that the number of C_{60} molecules inside the SWCNT has no significant effect on the Raman spectrum except on the RBLM mode which is the most sensitive to the degree of filling of the SWCNTs.

The dependence of the *VV* polarized Raman spectrum with the filling factor has been calculated for the $C_{60}@(10,10)$ and $C_{60}@(18,0)$ *linear peapods* [Figs. 5(a) and 5(c)] and the $C_{60}@(11,11)$ and $C_{60}@(13,13)$ *zigzag peapods* [Figs. 5(b) and 5(d)]. The spectra were calculated for five values of the filling factor $F=20\%$, 40%, 60%, 80%, and 100% corresponding to 4, 8, 12, 16, and 20 C_{60} molecules, respectively, inside SWCNT's. Figure 5 shows the filling factor dependence of the Raman spectrum in the BLM range.

For *linear peapods*, a single RBLM peak is calculated for empty tube (0%) and 100% filling factor. Let us call ω_h and ω_l the wave number of the 100% filling factor and empty tube, respectively. For small tube diameters, the increase of F from 0% to 100% leads to the appearance of two peaks at wave numbers close to ω_l and ω_h. The intensity of these peaks shifts from the one located around ω_l to that located around ω_h when increasing F. An illustration of a this behavior is shown for the $C_{60}@(10,10)$ peapod (tube diameter close of 1.36 nm) in Fig. 5(a). By contrast, for larger tube diameter, a single RBLM mode for all the filling levels is obtained. This behavior is displayed for the $C_{60}@(18,0)$ linear peapod, with tube diameter close to 1.41 nm in Fig. 5(c). The presence of a single RBLM is associated to the overlap of modes at ω_l and ω_h. Indeed, for linear peapods, we found that the difference $|\omega_h-\omega_l|$ varies from ~ 15 cm^{-1} for diameter around 1.26 nm to 0 cm^{-1} for diameter around 1.45 nm.

For *zigzag peapods*, and θ around θ_0, a double-peak struture appears when the filling factor increases as shown in the Raman spectrum of $C_{60}@(13,13)$ peapod [Fig. 5(d)]. By contrast, no significant change of the RBLM was observed for zigzag peapod systems when θ is close to 180° [$C_{60}@(11,11)$ peapod, for example, Fig. 5(b)] or θ close to 60° (not shown). Finally, we notice that, as expected, the intensity of the C_{60} $H_g(1)$ modes increases with the filling factor.

IV. DISCUSSION AND CONCLUSION

We have calculated the nonresonant Raman spectrum of isolated peapods. For the tube diameter investigated range, the C_{60} molecules adopt a linear arrangement for SWCNTs diameter lower than 1.45 nm, and a zigzag configuration for diameters between 1.45 nm and 2.20 nm. Both for the obtained *linear* and *zigzag peapods*, the dependence of the Raman spectrum with the diameter, the chirality and the nanotube filling level of the tube encasing C_{60}'s molecules chain have been analyzed. We found that the behavior of the RBLM mode with the SWCNT diameter was clearly modified in peapods. Therefore, the linear relation between the RBLM wave number and the inverse of diameter found in SWCNT will be modified in the peapod.

We can compare experimental data with the results of our calculations. Usually, experimental Raman spectra have been obtained on an ensemble of peapods organized in bundles.[6,26–28,40] Most of the peapod samples are featured by a diameter and chirality distributions. Due to the subtle effects on the RBLM and TLM induced by filling factor or change of the C_{60} configuration it is difficult to compare our predictions, calculated for individual peapods, with experimental data obtained on an ensemble of tubes in interaction. Nevertheless, Bandow *et al.* have found that the RBLM of the peapod having a tube diameter close to 1.37 nm [(10,10) SWCNT] was split in two components, downshifted and upshifted, respectively, with respect to the position of the RBM in empty SWCNT. Because the diameters involved is smaller than 1.45 nm, our calculations suggest that the RBLM splitting can be explained by a low C_{60} fullerene filling level inside SWCNTs.

Because experiments have been performed on peapod samples featured by diameter and chirality distributions, the

best way to test our predictions, is to focus on the behavior of C_{60} modes. Recently, Pfeiffer *et al.*[28] have performed a detailed Raman investigation on peapods organized in bundles. The temperature and excitation dependencies of the spectra have been analyzed. These authors focus on the dependence of the C_{60} modes in peapods. They found a splitting of the $A_g(1)$ and $A_g(2)$ modes of C_{60}. The components of the $A_g(1)$ are downshifted (490 cm^{-1}) and upshifted (502 cm^{-1}) with respect to the position of this mode in C_{60} (497 cm^{-1}). These results could be in agreement with our predictions. However, a spliting of the $A_g(2)$ mode was also observed. The components of the $A_g(2)$ mode are downshifted (1466 cm^{-1}) and upshifted (1475 cm^{-1}) with respect to the position of the $A_g(2)$ mode in C_{60} (1469 cm^{-1}). Such splitting of the $A_g(2)$ is not expected from our calculations. Consequently, we suggest that the splitting of $A_g(1)$ and $A_g(2)$ of C_{60} observed by Pfeiffer *et al.* are due to other origins of the filling factor or the zigzag configuration of C_{60} molecules inside the tube. We suggest that the results of Pfeiffer *et al.* can be understood by taking into account the presence of oligomers of C_{60} inside the tube. Recently, C_{60} oligomers (C_{60}'s covalently bonded by [2+2] cyclo-addition reaction) were identified in the same kind of peapods.[39] To confirm this assumption, calculations of the nonresonant Raman spectrum of peapods with oligomers of C_{60} inside the tube are in progress.

ACKNOWLEDGMENTS

The computations were performed at CINES (Montpellier, France). The work was supported by a CNRS-France/CNRST-Morocco agreement. One of the authors (H.C.) acknowledges the financial support from the CNRST-Morocco.

[1] H. W. Kroto, J. R. Heath, S. C. O'Brien, R. F. Curl, and R. E. Smalley, Nature (London) **318**, 162 (1985).
[2] S. Iijima, Nature (London) **354**, 56 (1991).
[3] N. Bendiab, R. Almairac, S. Rols, R. Aznar, J.-L. Sauvajol, and I. Mirebeau, Phys. Rev. B **69**, 195415 (2004).
[4] S. Rols, M. R. Johnson, P. Zeppenfeld, M. Bienfait, O. E. Vilches, and J. Schneble, Phys. Rev. B **71**, 155411 (2005).
[5] B. W. Smith, M. Monthioux, and D. Luzzi, Nature (London) **396**, 323 (1998).
[6] H. Kataura, Y. Maniwa, T. Kodama, K. Kikuchi, K. Hirahara, K. Suenaga, S. Iijima, S. Suzuki, Y. Achiba, and W. Krätschmer, Synth. Met. **121**, 1195 (2001).
[7] H. Kataura, Y. Maniwa, M. Abe, A. Fujiwara, T. Kodama, K. Kikuchi, H. Imahori, Y. Misaki, S. Suzuki, and Y. Achiba, Appl. Phys. A: Mater. Sci. Process. **74**, 349 (2002).
[8] Y. Maniwa, H. Kataura, M. Abe, A. Fujiwara, R. Fujiwara, H. Kira, H. Tou, S. Suzuki, Y. Achiba, E. Nishibori, M. Takata, M. Sakata, and H. Suematsu, J. Phys. Soc. Jpn. **72**, 45 (2003).
[9] S. Okada, S. Saito, and A. Oshiyama, Phys. Rev. Lett. **86**, 3835 (2001).
[10] R. F. Service, Science **292**, 45 (2001).
[11] Y. K. Kwon, D. Tomanek, and S. Iijima, Phys. Rev. Lett. **82**, 1470 (1999).
[12] J. Sloan, R. E. Dunin-Borkowski, J. L. Hutchiso, K. S. Coleman, V. C. William, J. B. Claridg, A. P. E. Yor, C. Xu, S. R. Baile, G. Brown, S. Friedrichs, and M. L. H. Green, Chem. Phys. Lett. **316**, 191 (2000).
[13] M. S. Dresselhaus and P. C. Eklund, Adv. Phys. **49**, 705 (2000), and related references therein.
[14] R. Saito, T. Takeya, T. Kimura, G. Dresselhaus, and M. S. Dresselhaus Phys. Rev. B **57**, 4145 (1998).
[15] A. Rahmani, J.-L. Sauvajol, S. Rols, and C. Benoit, Phys. Rev. B **66**, 125404 (2002).
[16] S. Rols, A. Righi, L. Alvarez, E. Anglaret, R. Almairac, C. Journet, P. Bernier, J.-L. Sauvajol, A. M. Benito, W. K. Maser, E. Munoz, M. T. Martinez, G. F. de la Fuente, A. Girard, and J.-C. Ameline, Eur. Phys. J. B **18**, 201 (2000).
[17] G. B. Adams, J. B. Page, O. F. Sankey, K. Sinha, J. Menendez, and D. R. Huffman, Phys. Rev. B **44**, 4052 (1991).
[18] J. H. Cho and M. H. Kang, Phys. Rev. B **51**, 5058 (1995).
[19] D. E. Weeks and W. G. Harter, J. Chem. Phys. **90**, 4744 (1989).
[20] Z. C. Wu, D. A. Jelski, and T. F. George, Chem. Phys. Lett. **137**, 291 (1987).
[21] G. Onida and G. Benedek, Europhys. Lett. **18**, 403 (1992).
[22] R. A. Jishi, R. M. Mirie, and M. S. Dresselhaus, Phys. Rev. B **45**, 13685 (1992).
[23] K. Hirahara, K. Suenaga, S. Bandow, H. Kato, T. Okazaki, H. Shinohara, and S. Iijima, Phys. Rev. Lett. **85**, 5384 (2000).
[24] M. Hodak and L. A. Girifalco, Phys. Rev. B **68**, 085405 (2003).
[25] M. Hodak and L. A. Girifalco, Phys. Rev. B **67**, 075419 (2003).
[26] S. Bandow, M. Takizawa, H. Kato, T. Okazaki, H. Shinohara, and S. Iijima, Chem. Phys. Lett. **347**, 23 (2001).
[27] S. Bandow, M. Takizawa, K. Hirahara, M. Yudasaka, and S. Iijima, Chem. Phys. Lett. **337**, 48 (2001).
[28] R. Pfeiffer, H. Kuzmany, T. Pichler, H. Kataura, Y. Achiba, M. Melle-Franco, and F. Zerbetto, Phys. Rev. B **69**, 035404 (2004).
[29] H. Ulbricht, G. Moos, and T. Hertel, Phys. Rev. Lett. **90**, 095501 (2003).
[30] *Light Scattering in Solids II*, edited by M. Cardona and G. Güntherodt (Springer-Verlag, Berlin, 1982).
[31] R. J. Bell, *Methods in Computational Physics* (Academic, New York, 1976), Vol. 15.
[32] S. Guha, J. Menendez, J. B. Page, and G. B. Adams, Phys. Rev. B **53**, 13106 (1996).
[33] C. Benoit, E. Royer, and G. Poussigue, J. Phys.: Condens. Matter **4**, 3125 (1992).
[34] J. Cambedouzou, V. Pichot, S. Rols, P. Launois, P. Petit, R. Klement, H. Kataura, and R. Almairac, Eur. Phys. J. B **42**, 31 (2004).
[35] X. Liu, T. Pichler, M. Knupfer, M. S. Golden, J. Fink, H. Kataura, Y. Achiba, K. Hirahara, and S. Ijima, Phys. Rev. B **65**, 045419 (2002).
[36] K. Hirahara, S. Bandow, K. Suenaga, H. Kato, T. Okazaki, H. Shinohara, and S. Iijima, Phys. Rev. B **64**, 115420 (2001).
[37] H. Kataura, T. Kodama, K. Kikuchi, K. Hirhara, K. Suenaga, S. Iijima, S. Suzuki, W. Kraetschmer, and Y. Achiba, in *AIP Con-*

ference Proceedings, edited by S. Saito, T. Ando, Y. Ywasa, K. Kikuchi, M. Kobayashi, and Y. Saito (AIP, Melville, NY, 2001), No. 590, p. 165.

[38] Ping Zhou, Kai-An Wang, Ying Wang, P. C. Eklund, M. S. Dresselhaus, G. Dresselhaus, and R. A. Jishi, Phys. Rev. B **46**, 2595 (1992).

[39] J. Cambedouzou, S. Rols, R. Almairac, J.-L. Sauvajol, H. Kataura, and H. Schober, Phys. Rev. B **71**, 041403(R) (2005).

[40] L. Kavan, L. Dunsch, H. Kataura, A. Oshiyama, M. Otani, and S. Okada, J. Phys. Chem. **17**, 7666 (2003).